15th Australasian Fluid Mechanics Conference
The University of Sydney, Sydney, Australia
13-17 December 2004

Dual-plane PIV investigation of structural features in a turbulent boundary layer

I. Marusic, B. Ganapathisubramani and E. K. Longmire

Department of Aerospace Engineering & Mechanics
University of Minnesota, Minneapolis, MN 55455, USA

Abstract

Simultaneous dual-plane PIV experiments were performed in streamwise-spanwise planes in the log region of a turbulent boundary layer at a moderate Reynolds number ($Re_\tau \sim 1100$). The acquired datasets were used to resolve all 9 velocity gradients from which the complete vorticity vector and other invariant quantities like 3-D swirl strength were computed. These derived quantities were used to analyze and interpret the structural characteristics and features of the boundary layer. Results of the vorticity vector and the 2-D swirl strength from the two neighbouring planes indicate the existence of hairpin shaped vortices inclined downstream along the streamwise direction. These vortices envelop low speed zones and generate Reynolds shear stress that enhances turbulence production. Plots of full 3D swirl strength indicate the existence of additional vortical structures in the middle of the low speed zones that may represent heads of smaller eddies intersecting the measurement plane. This concept is in accordance with the hierarchy of structure size in a hairpin packet proposed by Adrian *et al.*[2]. Computation of inclination angles of individual eddies using the vorticity vector suggests that most cores are inclined at 25° to the streamwise-spanwise plane with a resulting projected eddy inclination of 32°.

Introduction

Over the past few decades, researchers have worked toward understanding the eddy structure within turbulent boundary layers in order to develop effective simplifying models. Recently, Adrian *et al.* [2] have reinforced the viewpoint that "hairpin vortices" are a primary feature in turbulence transport and production. The authors performed PIV experiments in streamwise-wall-normal planes of a turbulent boundary layer and found instantaneous signatures of heads of hairpin vortices. Most significantly, they observed that these vortices travelled together in spatially coherent groups, termed "hairpin packets". Recently, Ganapathisubramani *et al.* [5], with stereoscopic PIV data in streamwise-spanwise planes, concluded that these hairpin packets occupy only a small percentage of the total area in the log layer, but contribute a significant proportion of the total Reynolds shear stress generated, conservatively more than 30%. Therefore, the hairpin packets are a very important mechanism in turbulence production. However, a detailed understanding of the three dimensional structure of hairpin vortices and packets is not yet available, and many questions regarding the shape, size, orientation and dynamics or these structures remain unanswered. The objective of the current experimental study is to obtain the full velocity gradient tensor over a plane in order to begin answering these questions.

Experiment and methods

Experiments were performed in a suction type boundary layer wind tunnel. Measurement planes were located 3.3 m downstream of a trip wire in a zero-pressure-gradient flow with freestream velocity U_∞ = 5.3 m s^{-1} and Re_τ = 1060 ($Re_\tau = \delta U_\tau/\nu$, where δ is the boundary layer thickness, U_τ is the skin friction velocity). All measured flow parameters shown in the results section are normalized using the skin friction velocity (U_τ) and kinematic viscosity (ν) and are denoted with a superscript +. The streamwise, spanwise and wall-normal directions are along the *x*, *y* and *z* axes respectively.

Two independent PIV systems capture data simultaneously in neighboring streamwise-spanwise planes separated by $\sim$ 1 mm (15 wall units) as shown in figure 1. System 1 is a stereoscopic system used to provide all three velocity components over a plane illuminated by Sheet 1, and System 2 is a single-camera planar PIV system. The single-camera system measures the streamwise-spanwise velocity components in the higher plane illuminated by Sheet 2. Simultaneous measurements are performed utilizing the polarization property of the laser light sheets to isolate one plane to one set of camera/cameras (see e.g. [9, 8, 3]). PIV data were captured in the log layer region of the turbulent boundary layer.

System 1 includes two TSI Powerview $2k \times 2k$ pixel resolution cameras equipped with Nikon 50 mm lenses. The lenses are fitted with linear polarizers oriented to allow the passage of horizontally polarized light only. Light sheets for System 1 are generated by a pair of Nd:YAG lasers (120 mJ/pulse) that are horizontally polarized. System 2 includes one TSI Powerview camera with $2k \times 2k$ pixel resolution and a Nikon 50 mm lens. The linear polarizers in this case are oriented to allow the passage of vertically polarized light only. The illumination source for System 2 is a pair of Nd:YAG (120 mJ/pulse) lasers of vertical polarization. The laser pairs in Systems 1 and 2 are aligned independently to illuminate a specific wall-normal location. The timing of each laser/camera system is controlled using a TSI synchronizer box. In order to ensure simultaneous capture of images, an external trigger is provided to both synchronizer boxes for image capture at a frequency of 0.2 Hz. The data from the two systems are streamed continuously to disk.

Vector fields are computed using a 32×32 pixel window in both planes. The vectors from each camera in the stereo plane are then combined using suitable magnification factors to compute all three velocity components (see [4]). The vector field from the single camera is resampled and mapped to the grid of the stereo measurement using bi-linear interpolation. The resolution of the resulting vector fields is about 18×18 wall units, and the total field size is $1.8\delta \times 1.8\delta$.

The single camera vector fields from the upper plane in liaison with the stereoscopic data from the lower plane are then used to compute all velocity gradients in the lower plane. A second order central difference method is used to compute all possible in-plane gradients while a first order forward difference is used to compute the wall-normal gradients of the streamwise and spanwise velocities. Finally, the continuity equation is used to recover the wall-normal gradient of the wall-normal velocity. With the out-of-plane gradients provided by the dual-plane data, we are able to compute the complete swirl strength and vorticity vector.

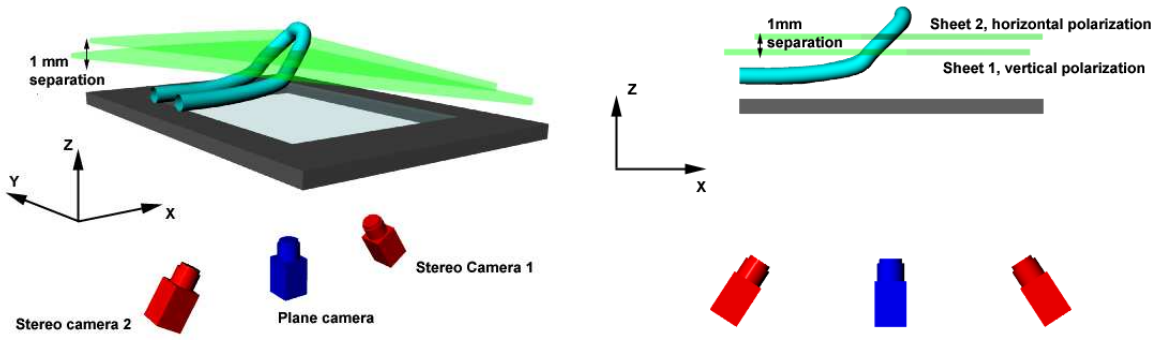

(a) (b)

Figure 1: (a) Perspective view (b) side view of the experimental setup

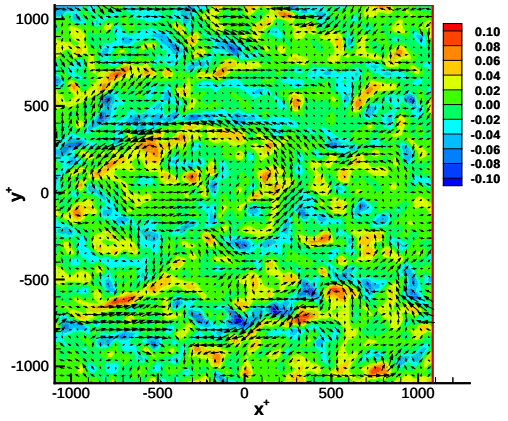

(a)

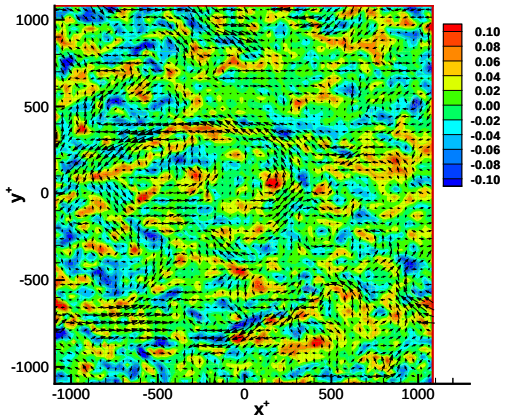

(b)

Figure 2: Vorticity components at $z^+ = 125$ (a) ω_z^+, (b) ω_x^+. The flow is from left to right and the vectors shown have the mean streamwise velocity ($\overline{U}$) subtracted.

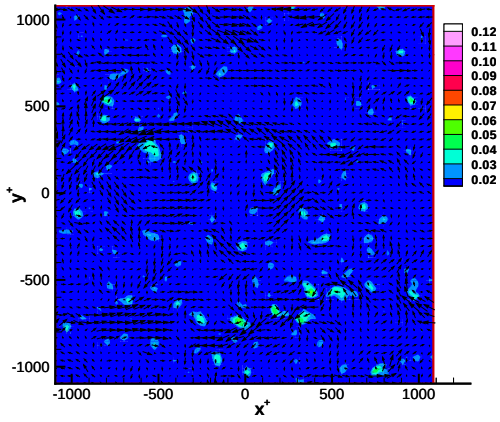

(a)

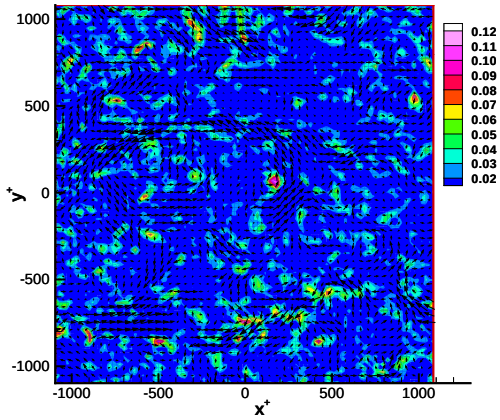

(b)

Figure 3: Swirl strength at $z^+ = 125$ (a) λ_{2D}^+ and (b) λ_{3D}^+. The flow is from left to right and the vectors shown have the mean streamwise velocity ($\overline{U}$) subtracted.

Results and Discussion

Examination of streamwise and spanwise velocities from the lower and upper planes reveals that the two planes are very well correlated. At this wall-normal position ($z^+ = 125$) the streamwise velocity signature is typically seen to contain long low and high speed regions bordering one another in the spanwise direction. A typical field is shown in figures 2 and 3.

Contours of wall-normal vorticity (ω_z^+, figure 2(a)) show that, in this orientation, the tops of low speed regions are typically enveloped by negative values and the bottoms by positive values. Also, the variations in vorticity strength seem to indicate that these regions of vorticity contain swirling motions indicative of vortex cores. These cores are noted as being predominantly inclined to the plane. This point becomes clear from the streamwise vorticity ω_x^+ plot (figure 2(b)). The regions of positive ω_z^+ have predominantly positive ω_x^+, and regions of negative ω_z^+ have negative ω_x^+. The data thus are consistent with the presence of vortices inclined at an angle with respect to the streamwise direction. We will refer to these inclined vortices broadly as hairpin vortices, which may or may not be symmetric. Note, however, that inclined hairpins are not the only type of instantaneous structures observed. Examination of various vector fields in the two neighbouring planes indicate evidence of some structures that are inclined at 90 degrees to the streamwise direction and others that are completely streamwise.

Figure 3(a) reveals the instantaneous two dimensional swirl strength (λ_{2D}^+) at $z^+ = 125$. Two dimensional swirl strength is computed from the eigenvalues of the in-plane (2-D) velocity gradient tensor (see [1]) and is the measure of the swirling tendency of the flow. This plot in tandem with ω_z^+ (see figure 2(a)) shows that 2-D swirl isolates regions that are swirling about an axis aligned with the wall-normal direction. A visual comparison between the swirl in the lower and upper planes (not shown here) indicates a forward tilt to most structures as they are offset in the positive streamwise direction in the upper plane. It should be noted that λ_{2D}^+ cannot identify vortices whose inclination angles to the plane are small. Figure 3(b) presents a plot of the full swirl strength (λ_{3D}^+, computed from the eigenvalues of the complete 3-D velocity gradient tensor [10]). The plot reveals that the 3-D swirl identifies not only the vortices cutting across the plane but also additional regions that are not isolated by 2-D (wall normal) swirl. These regions could possibly coincide with smaller hairpin vortices whose heads are cutting across the measurement volume and hence are not apparent in the 2-D swirl plot.

Having the full three-dimensional information in a plane, it is now possible to study the inclination angle of vortex structures by computing the orientation of the vorticity vector. If the vector angle is computed at every point in the field, the results are noisy partly due to measurement uncertainty, but primarily due to the predominance of small-scale incoherent motions to the instantaneous vorticity, and thus the instantaneous vortex lines in a turbulent flow are not very well organized. By contrast, computation of the vorticity vector averaged over a region identified as a vortex core by the swirl strength λ_{3D}^+, leads to determination of the orientation of the vortex core. This orientation can then be interpreted as the local inclination of that vortex.

Figure 4(a) reveals the probability density function (p.d.f.) of the inclination angle (θ_e) that vortex cores make with the $x-y$ plane. The angles were computed for all distinct regions of significant λ_{3D}^+. This distribution (square symbols) includes a wide range of structure angles at this wall-normal location. Note that many structures have small inclination angles. Further study, including the investigation of the azimuthal angle made by the projection of the vorticity vector onto the $x-y$ plane with the

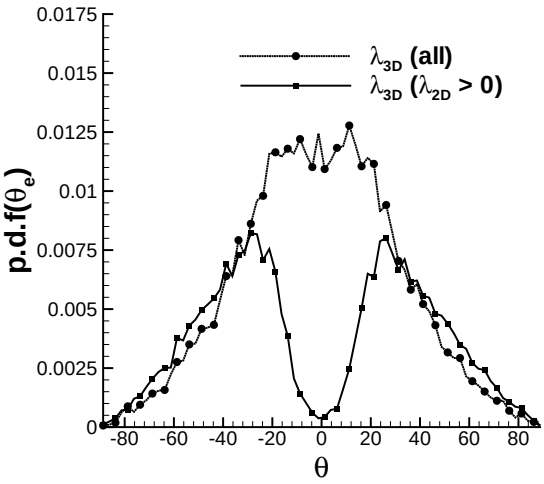

(a)

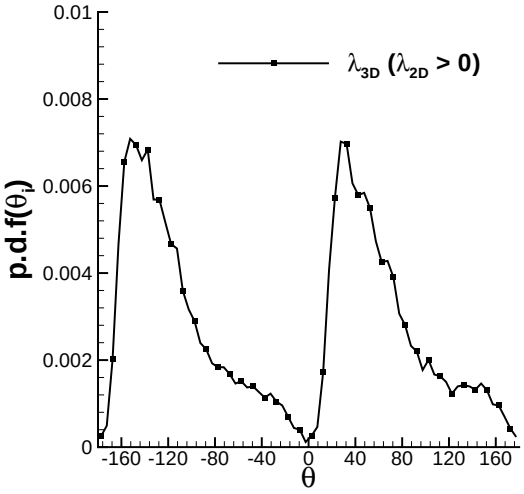

(b)

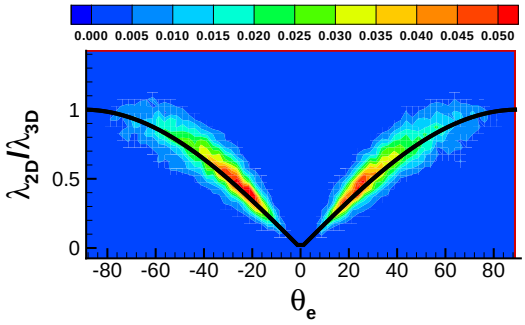

(c)

Figure 4: p.d.f. of (a) Inclination angle (θ_e), (b) Eddy inclination angle (θ_i), (c) Joint p.d.f of inclination angle and $\lambda_{2D}/\lambda_{3D}$, the solid line is the function $\lambda_{2D}/\lambda_{3D} = |\sin\theta_e|$.

x axis, reveals that most λ_{3D}^{+} regions with small inclinations are spanwise structures indicative of heads of smaller hairpin vortices or other in-plane oriented vortices. In order to obtain the inclination angles of cores that are not spanwise heads or streamwise legs, the average vorticity vector in isolated regions of λ_{3D}^{+} that includes λ_{2D}^{+} were computed. This additional criterion filters out spanwise and streamwise structures since λ_{2D}^{+} does not capture them. The resulting p.d.f., shown by circles in figure 4(a)) yields peaks at $\pm 25^{\circ}$. This suggests that most cores are inclined at 25° to the $x-y$ plane. The angle made by the projection of the vorticity vector in the $x-z$ plane with the x axis is defined as the eddy inclination (θ_i). The p.d.f. of the eddy inclination angle (only for regions where $\lambda_{2D}^{+} > 0$) is shown in figure 4(b). This p.d.f has peaks at $\pm 32^{\circ}$, which indicates that most of the inclined vortex rods have an inclination of 32°. This is comparable to a 45° hairpin inclination as suggested by various researchers over the past century ([7]). Another measure is the weighted average of θ_e and θ_i based on the centre of area of the p.d.fs shown in the figures respectively. This reveals that the average inclination angle θ_e is 37° and the average eddy inclination (θ_i) is 57° at this wall-normal location.

Figure 4(c) is a plot of the joint probability distribution of the ratio of 2-D swirl strength to 3-D swirl strength and the inclination angle (θ_e). It is worth noting that, mathematically λ_{2D} will always be less than or equal to λ_{3D} for any orientation. The distribution indicates a unique relationship between this ratio and the inclination angle of vortex structure with respect to the cutting plane ($x-y$ plane in this instance). Velocity fields induced around idealized hairpin vortices (with and without curvature) were computed using Biot-Savart calculations to calculate the ratio $\lambda_{2D}/\lambda_{3D}$ as a function of the hairpin angle. The results from this computation suggest that the ratio of the two swirl strengths varies as $|\sin\theta_e|$. The value of this ratio from the experiments follows this theoretical finding as seen in figure 4(c). Note that this plot does not reveal any information about the streamwise or spanwise oriented structures, since the ratio was computed only for cores where λ_{2D} is greater than zero. The fact that the distribution is dense in the angle range $20^{\circ} < \theta_e < 40^{\circ}$ indicates that most vortex structures in this plane are inclined in that range of angles.

Conclusions

Simultaneous dual-plane PIV experiments were successfully performed to compute all nine velocity gradients in a turbulent boundary layer. Dual-plane measurements could be used to compute the complete vorticity vector and other quantities like instantaneous Reynolds shear stress production and 3-D swirl strength to study the eddy structure and their dynamics. Contours of different components of the vorticity vector and 2-D swirl strength from the two neighboring planes indicate the existence of hairpin shaped vortices inclined downstream along the streamwise direction. These vortices envelop low speed zones and generate Reynolds shear stress that enhances turbulence production (see [6]). Plots of 3-D swirl strength indicate the existence of additional vortical structures in the middle of low speed zones that may represent heads of smaller eddies intersecting the measurement plane. The dual-plane data were also used to compute typical vortex inclination angles at this wall-normal location. It is worth noting that this study includes just one dataset at one wall-normal location. Datasets at multiple wall-normal locations are required to resolve the complete vortex structure and earn more about the dynamics of a turbulent boundary layer.

Acknowledgements

The authors gratefully acknowledge support from the National Science Foundation through Grants ACI-9982274, CTS-9983933 and CTS-0324898, the Graduate school of University of Minnesota and the David and Lucile Packard Foundation. We are indebted to Dr. Nicholas Hutchins and William Hambleton for their help in data acquisition and many discussions during the course of this study.

References

[1] Adrian, R. J., Christensen, K. T. and Liu, Z. C., Analysis and interpretation of instantaneous turbulent velocity fields, *Exp. Fluids*, **29**, 2000, 275–290.

[2] Adrian, R. J., Meinhart, C. D. and Tomkins, C. D., Vortex organization in the outer region of the turbulent boundary layer, *J. Fluid Mech.*, **422**, 2000, 1–53.

[3] Christensen, K. T. and Adrian, R. J., Measurement of instantaneous eulerian acceleration fields by particle image accelerometry: method and accuracy, *Exp. Fluids*, **33**, 2002, 759–769.

[4] Ganapathisubramani, B., Longmire, E. K. and Marusic, I., Investigation of three dimensionality in the near field of a round jet using stereo PIV, *J. Turbulence*, **3**, 2002, 017.

[5] Ganapathisubramani, B., Longmire, E. K. and Marusic, I., Characteristics of vortex packets in turbulent boundary layers, *J. Fluid Mech.*, **478**, 2003, 35–46.

[6] Ganapathisubramani, B., Longmire, E. K., Marusic, I. and Pothos, S., Dual-plane PIV technique to resolve complete velocity gradient tensor in a turbulent boundary layer, in *12th International Symposium of Applications of Laser Techniques in Fluid Mechanics*, Lisbon, Portugal, July 12-15, 2004.

[7] Head, M. R. and Bandyopadhyay, P., New aspects of turbulent boundary-layer structure, *J. Fluid Mech.*, **107**, 1981, 297–337.

[8] Hu, H., Saga, T., Kobayashi, T., Taniguchi, N. and Yasuki, M., Dual-plane stereoscopic particle image velocimetry: system set-up and its application on a lobed jet mixing flow, *Exp. Fluids*, **31**, 2001, 277–293.

[9] Raffel, M., Willert, C. and Kompenhans, J., *Particle image velocimetry - A practical guide*, Springer-Verlag, 1998.

[10] Zhou, J., Adrian, R. J., Balachandar, S. and Kendall, T. M., Mechanisms for generating coherent packets of hairpin vortices in channel flow, *J. Fluid Mech.*, **387**, 1999, 353–396.